DOR: 20.1001.1.2322388.2021.9.2.4.2

Research Paper

Robust Multi-Objective Optimization of Mechanical Properties of Friction Stir Welding Using Neural Network and Modified-NSGA-II

Mostafa Akbari*, Hossein Rahimi Asiabaraki

Department of Mechanical Engineering, Technical and Vocational University (TVU), Tehran, Iran

ARTICLE INFO

Article history:

Received 25 February 2021
Accepted 18 April 2021
Available online 1 May 2021

Keywords:
Friction stir welding
Optimization
Robust
Neural Network

ABSTRACT

In this paper, the optimal parameters of the FSW welding process to improve the joint's mechanical properties are obtained using robust multi-objective optimization. First, the properties of the weld zone, such as the chemical composition of the weld, are investigated using scanning electron microscopy (SEM) and energy-dispersive X-ray spectroscopy (EDS). The hardness and tensile properties of the weld were investigated to evaluate the mechanical properties of the joint. The results show at the AA7075 side, the highest hardness is observed in the TMAZ, and the hardness is reduced in the SZ. Tensile testing revealed that the joint's mechanical characteristics were superior to those of the basic metals. In order to obtain the relationship between the process input parameters and the mechanical properties of the obtained joint, an artificial neural network model (ANN) was used. The relationship obtained by ANN was then used to obtain the optimal values of process parameters considering uncertainties in a robust optimization algorithm. In this way, using such an obtained feed-forward neural network and the Monte Carlo simulation, a multi-objective genetic algorithm is used for the robust Pareto optimization of the friction stir welding parameters having probabilistic uncertainties in parameters. Finally, the Technique for Order Preference by Similarity to the Ideal Solution (TOPSIS) was used to get the best optimum solution. The robust optimal process parameters were determined by robust multivariate optimization to be 1467 rpm rotational speed and 11 mm/min traverse velocity.

* **Corresponding Author**:
E-mail Address: mo-akbari@tvu.ac.ir

1. Introduction

In 1991, friction stir welding (FSW) was introduced as a relatively new technology for joining alloys that are difficult to weld using standard methods. Since the introduction of this method, many investigations have been conducted to develop this method in various applications, such as the automotive industry. Friction stir welding has been employed to join different alloys such as aluminum [1, 2], Mg [3-5], and Cu [6, 7]. In this method, a non-consumable tool generates heat and softens the material, thus creating a flow of material. So far, this method has been used successfully to join different dissimilar metals [8, 9]. Han et al. [10] evaluated the mechanical characteristics for friction stir welding of 5083-O Al alloy. This study introduced the optimal process parameters for the rotational speed of 800 rpm and the traverse velocity of 124 mm/min. Amancio-Filho et al. [11] friction stir welded dissimilar Al alloys (AA2024-T351 and AA6056-T4). Their tensile testing has shown that strength is up to 90% of the weakest joining partner 6056-T4. Ghiasvand et al. [12] investigated the effects of three FSW parameters on the maximum temperature of FSW of AA5086 and AA6061 alloys. Their results illustrated that pin offset is the most influential parameter affecting maximum temperature during the process. Yuvaraj et al. [9] optimized parameters of the FSW tool for welding dissimilar AA6061 and AA7075-T651 aluminum alloys using the Taguchi method. Verma et al. [13] evaluated the optimization of friction stir welding parameters of dissimilar aluminum alloys 6061 and 5083 using response surface methodology. They investigated the effect of varying tool rotational speed, tool traverse speed, tool pin shape, and tool tilt angle on the tensile strength and elongation. As it turns out, optimization of process parameters has been the focus of researchers in recent years to achieve better joint. So far, various methods have been used to achieve optimal process values, some of which have been mentioned. In this research, a new method, considering uncertainties, was used in order to obtain the optimal process parameters.

In real engineering practices, there are different causes of uncertainty, such as imperfect parameter knowledge, parameter fluctuations owing to environmental circumstances, and so on, which must be compensated by an optimal robust design strategy [14]. Uncertainties have not been considered in traditional optimization methods that researchers have used to optimize process parameters, and the optimization is done deterministically. Without addressing uncertainty, generally non-optimal and potentially high-risk solutions were obtained. As a result, finding a robust design with low-performance fluctuation in the presence of uncertainties is very desirable. In general, a method named robust design optimization (RDO) is used to handle the stochastic robustness issue [14].

In this paper, the mechanical properties of the friction stir welding of AA7075-O to AA5083-O aluminum alloys were investigated. An artificial neural network was constructed to model the correlation between the friction stir welding parameters and mechanical properties using data obtained from experimental. Finally, a robust multi-objective optimization strategy employing MCS was employed to discover the best possible traverse and rotational speed combination to provide the optimal combination of hardness and tensile qualities.

2. Materials and Methods

This study used two different rolled plates of aluminum alloys, AA7075-O and AA5083-O. Table 1 lists the chemical compositions of the rolled plates, which were 6 mm thick. Fig. 1 depicts the use of friction stir welding.

Fig. 1. Welding tool utilized in this investigation

Table 1. Chemical composition of alloys

Weight (%)	Si	Fe	Cu	Mn	Mg	Zn	Ti
AA7075	0.27	0.36	1.21	0.02	1.74	4.9	0.033
AA5083	0.40	0.40	0.1	0.2	0.4	0.1	0.15

SEM and EDS were used to examine the chemical characteristics of the welding zone. The Vickers microhardness test was done with a force of 100 g and a dwell period of 15 seconds at a distance of 3 mm from the top surface of the samples. Room-temperature tensile tests were conducted on samples as per ASTM E8 [15] on a tensile testing machine.

After performing microstructural and mechanical tests, optimal parameters will be obtained using a robust multivariate optimization method (Fig. 2). In order to use optimization algorithms, it is necessary to determine a mathematical relationship between the input parameters and the output performance of the process. For this purpose, an artificial neural network was employed to determine this mathematical relationship. Then, to tackle this robust multi-objective optimization problem, a hybrid robust multi-objective optimization was adopted. This method is divided into two stages: modified-NSGAII develops a Pareto front, and TOPSIS selects the optimum solution for the Pareto front.

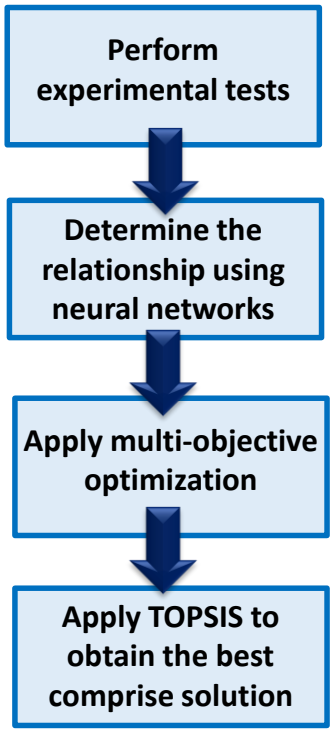

Fig. 2. The procedure of the proposed approach

3. Experimental Results

3.1. Microstructural and SEM-EDS analysis of the welded joints

Fig. 3a and c illustrate the microstructures of the base alloys of AA7075 and AA5083, respectively. Because of the concentration of small precipitates in grain boundaries, the grains in AA7075 were highly characterized. As shown in Fig. 3b, the grains in the SZ are much finer than the base metal due to the recrystallization of the grains in this region. Severe plastic deformation and frictional heat generated in friction stir welding create a microstructure with recrystallized coaxial grains within the stir zone [16].

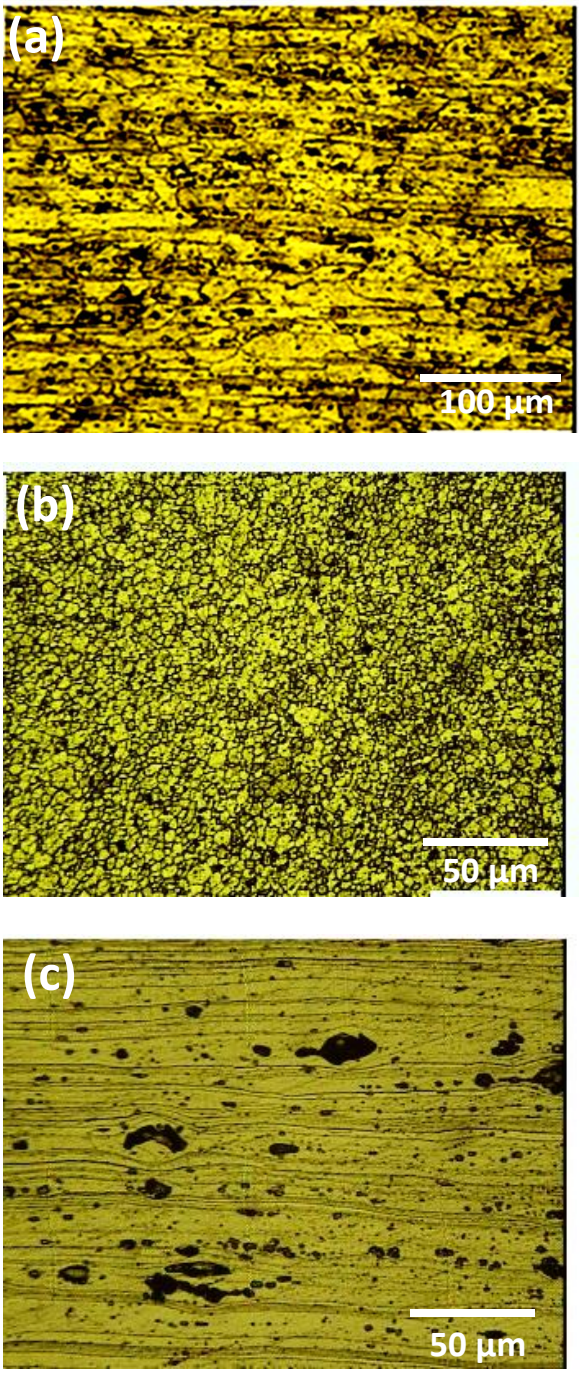

Fig. 3. Microstructures of (a) AA7075 base alloy and (b) stir zone of the weld, (c) AA5083 base alloy.

The EDS analyses were done on some points in the interface between AA7075 and AA5083. The EDS results at these points were similar to each other. Therefore, it can be concluded that the composition of the interface between AA7075 and AA5083 is uniform. The EDS analysis of one of these points (the point B of the interface between AA7075 and AA5083) has been shown in Fig. 4. As an example, the mass percentages of Cu, Zn, and Mg at the position of A almost corresponded to the content of 7075 alloys, while the concentration of Mg and Mn at the position of C was close to 5083 Al alloy plate. At point B, the mass percentages of Mg, Mn, Cu, and Zn were the average of two base materials; we could assert by this time that this point was the interface of mixed two materials; we could assert by this time that this point was the of the mixed two materials. In order to get the best and most certain results for the welded joint, a Line-Scan interface analysis was done (Fig. 5). The Line-Scan interface analysis demonstrated that the mass percentage of Mg was increased while moving from the advancing side to the retreating one

and in the weld nugget was average. On the other hand, the mass value of Zn corresponding to the content of 7075 alloys was reduced. This analysis method was used to graphically show each alloying element in the weld center and the concentration of each alloying element in the weld sample. This investigation noted that the distribution of the alloying elements in the weld center was heterogeneous, and the difference in various properties between the welded joint and the base material was clearly proved.

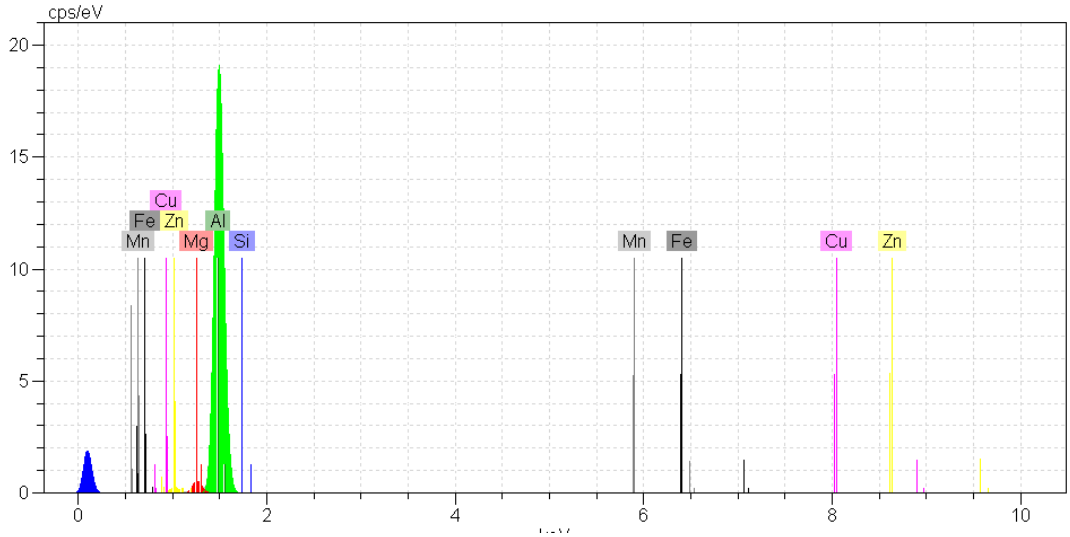

Fig. 4. EDS quantitative analysis of interface between AA7075 and AA5083 corresponding to point B

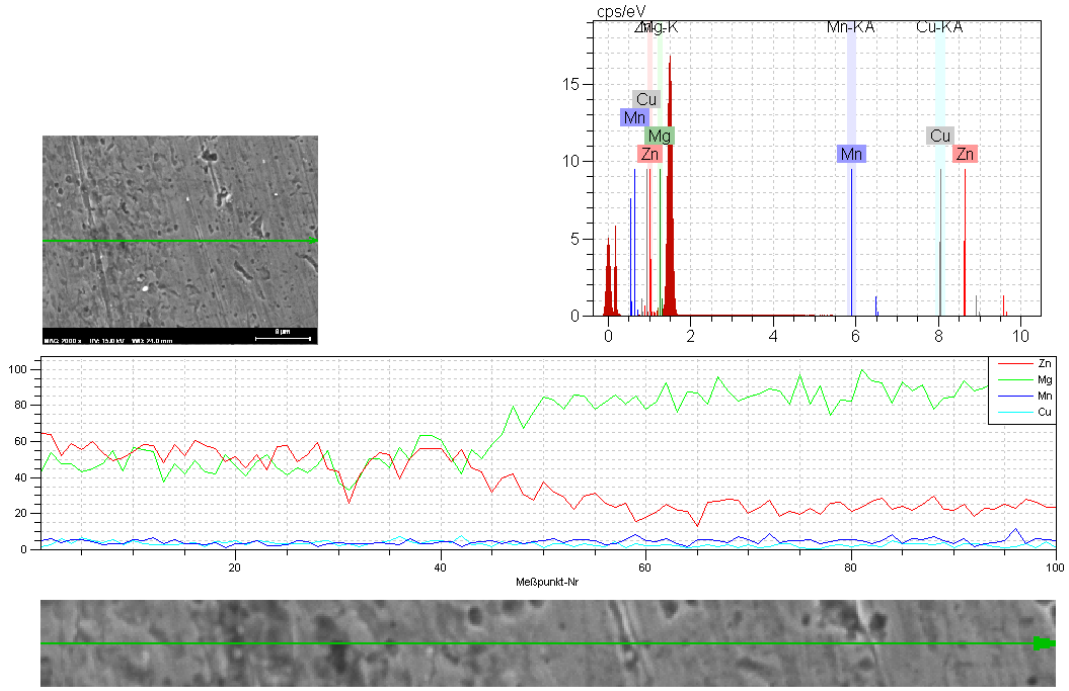

Fig. 5. Line-Scan analysis of the welded sample

3.2. Hardness and tensile tests

Hardness variation in the cross-section of the welded specimen produced at a rotational speed of 700 rpm and a linear velocity of 36 mm/min can be seen in Fig. 6 [11]. As it is known, on the AA7075 side, the highest hardness is observed in the TMAZ and the HAZ, and the hardness is reduced in the SZ region. It is worth noting that the hardness of the SZ is still higher than the base metal. The hardness changes in the AA5083 processed zone are very small, and the hardness in the weld zone is slightly higher than in the base metal. Because strain hardening is the predominant hardening mechanism in 5083 alloys, the hardness profile in this zone was mostly influenced by dislocation density.

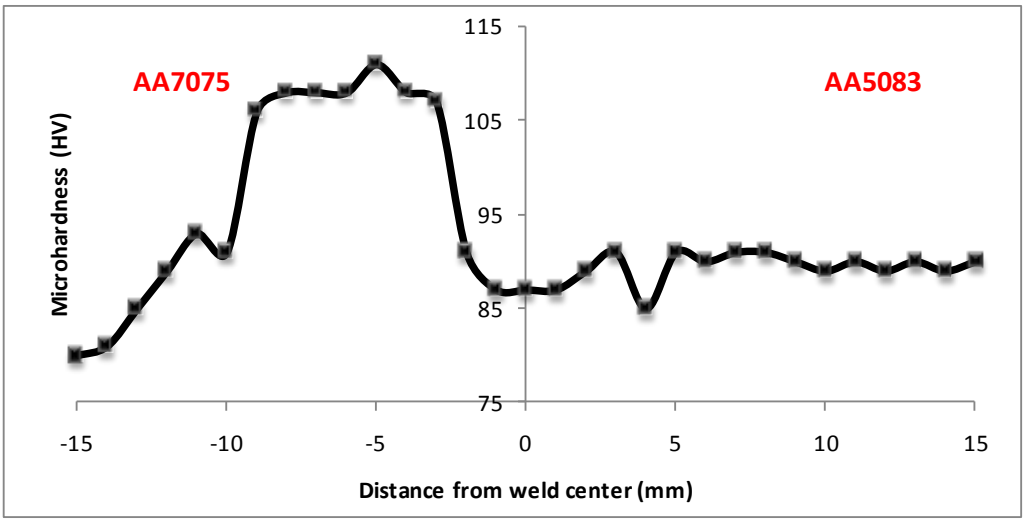

Fig. 6. Microhardness profile of the joint

Table 2 shows the different hardness and tensile strength values of welded specimens using different rotational and traverse velocities [17]. As is evident at all traverse velocities, increasing the rotational speed increases the tensile strength values. As the rotational speed increases, the strain applied by the tool to the material increases, resulting in better and stronger mixing between the materials. On the other hand, reducing the linear velocity increases the tensile strength of welded specimens. Reducing the traverse velocity causes the materials to be affected by strain for a longer time, resulting in better mixing [18, 19].

Furthermore, high welding speeds result in low generated temperature and material deformation, resulting in the production of an unsound joint. The hardness of the specimens decreases with increasing rotational speed or decreasing linear velocity. The heat input to the workpiece increases as the rotating speed increases or traverse speed decreases during welding, which promotes grain growth and consequently decreases hardness (Table 2).

Table 2. Hardness values and tensile strength of welded specimens using different parameters

No	Traverse Speed (mm/min)	Rotational Speed (rpm)	Tensile Strenght (Mpa)	Hardness (HV)
1	20	565	198	97.9
2	36	565	177	97.3
3	63	565	161	95.2
4	96	565	142	92.89
5	20	700	192	96.7
6	36	700	180	95.25
7	63	700	165	90.9
8	96	700	148	91.67
9	20	900	216	93.7
10	36	900	192	94.1
11	63	900	173	91
12	96	900	150	90.1
13	20	1200	232	94.2
14	36	1200	201	92.1
15	63	1200	180	90.1
16	96	1200	154	88.23
17	20	1400	267	92.3
18	36	1400	221	90.23
19	63	1400	195	89
20	96	1400	171	87.21

4. Modeling using neural networks

In this research, a feed-forward neural network with a back-propagation algorithm has been used to extract the relationship between process input parameters, i.e., linear velocity and tool rotational speed, and output parameters, i.e., hardness and tensile strength. Also, the input and output values of the experimental results were normalized in the range of 0-1 for use in the neural network. Proper selection of neural network architecture is necessary to increase the accuracy of the neural network. For this purpose, several neural networks with different architectures were evaluated, and the best architecture was selected based on trial and error. Based on this analysis, a neural network with six neurons in the hidden layer and the "logsig" function were used. In order to train the neural network, 80% of the experimental data was randomly selected, and the remaining 20% was used for network testing. At the training and testing stages, the correlation coefficients for ultimate tensile strength and hardness were 0.9999 and 0.9916 and 0.9799 and 0.9891, respectively. As it turns out, the performance of the neural network in predicting process outputs is excellent.

The following equations (9-11) were extracted from the ANN to determine tensile strength and hardness:

$$\text{UTS} = \left(\frac{1}{1+e^{-(-1.447\times F_1+0.390\times F_2-0.497\times F_3+0.055\times F_4+0.415\times F_5-0.331\times F_6+2.14)}}\right) \quad (1)$$

$$Hardness = \left(\frac{1}{1+e^{\left(-(-0.198\times F_1+0.169\times F_2-0.0762\times F_3-0.303\times F_4+0.281\times F_5+0.080\times F_6+1.86)\right)}}\right) \quad (2)$$

where $F_{(i = 1, 2, 3, \dots, 6)}$ can be calculated using:

$$F_i = \frac{1}{1+exp^{-U_i}} \quad (3)$$

$$U_i = C_{1i} \times R + C_{2i} \times T + C_{3i} \quad (4)$$

where

U_1 to U_6 may be determined as follows:

Constants, Cji, in Equation (4), are illustrated in Table 2. T and R are traverse and rotational speeds, respectively. T and R are traverse and rotational velocities, which are normalized by dividing them by 1600 and 100, respectively, in this equation. Hardness and ultimate tensile strength must be multiplied by 110 and 300, respectively, for outputs.

Table 3. Weights and biases between the input layer and hidden layer for Equations (1) and (2).

$U_i = C_{1i} \times R + C_{2i} \times T + C_{3i}$			
i	C_{1i}	C_{2i}	C_{3i}
1	50.53	-58.73	34.21
2	-30.54	23.086	1.76
3	-45.85	-13.57	54.87
4	2.95	62.84	-48.98
5	10.32	-51.71	25.50
6	13.17	-233.73	107.30

5. Robust analysis

Robust optimization is an engineering methodology for obtaining optimal process parameters that are less sensitive to process variations. Excessive performance variations result in decreasing product quality. This highlights the need for robust design. One way to reduce performance variations caused by uncertainties is to find solutions where the performance is less sensitive to parameter variations without eliminating the cause of the changes, as in robust optimization.

The concept of robustness can be seen schematically in Fig. 7. In this figure, the value of a function *f* must be maximized. When the system parameters are randomly perturbed from their nominal values, the two curves represent the distributions of the occurrence frequency of the value of f corresponding to two individual designs. In the figure, μ_1 and μ_2 state the mean values of the function *f* for the two designs, respectively. Even though the second design has a greater mean value of the cost function, the first design is preferred in terms of robustness since it is significantly less sensitive to changes in the unknown system characteristics [14].

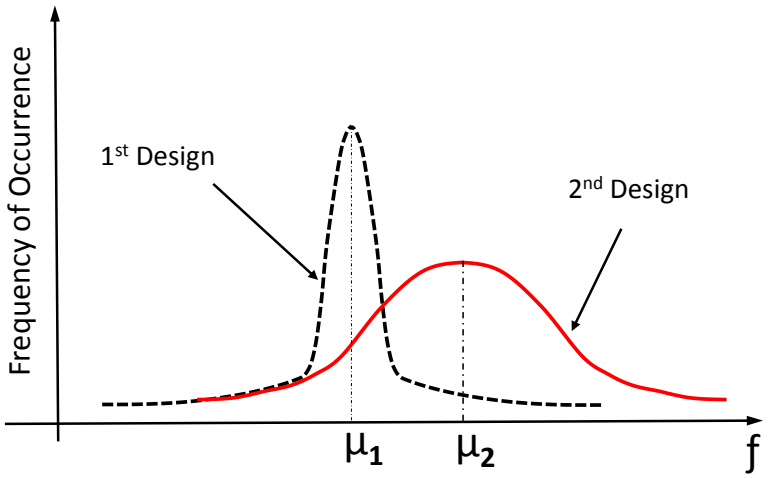

Fig. 7. Concept of robust design

The idea underlying robust optimization is that the best process parameter is justified not only by its mean value but also by its variability in performance. One straightforward way of optimizing process parameters is to define the optimality conditions of the problems based on the deterministic value of the function [17]. However, this ideal design may still be susceptible to changes in the parameters, which presents the issue of design robustness [20].

Consider *X* as a random variable, then the prevailing model for uncertainties in stochastic randomness is the probability density function *(PDF), f(x)* or equivalently by the cumulative distribution function *(CDF), F(x),* where the subscript X refers to the random variable. This can be given by

$$F_x(x) = \Pr(X \le x) = \int_{-\infty}^{x} f_x(x)dx \tag{5}$$

where Pr(X ≤ x) is the probability that an event (X ≤ x) will occur. Some statistical moments such as the first and the second moment, generally known as mean value (also referred to as expected value) denoted by $\mu(X)$ and variance denoted by $\sigma^2(X)$, respectively, are the most important ones. They can also be computed by:

$$\mu(X) = \int_{-\infty}^{\infty} x dF_X x = \int_{-\infty}^{\infty} x f_x(x)dx \tag{6}$$

And

$$\sigma^2(x) = Var(X) = \int_{-\infty}^{\infty} (x-\mu(X))^2 dF_x(x) = \int_{-\infty}^{\infty} (x-\mu(X))^2 df_x(x) \tag{7}$$

These equations can be easily expressed in the case of discrete sampling as:

$$\mu(X) \cong \frac{1}{N}\sum_{i=1}^{N} x_i \tag{8}$$

And

$$\sigma^2(X) = Var(X) \cong \frac{1}{N-1}\sum_{i=1}^{N} (x_i - \mu(X))^2 \tag{9}$$

where x_i is the *ith* sample and *N* is the total number of samples.

In robust optimization, the goal is to reduce process variability caused by unknown probabilistic factors describing deterministic behavior. As a result, the problem of robust optimization can be expressed as follows:

$$\begin{aligned} &\text{Minimize } \{\mu[f(x,d,p)], \upsilon[f(x,d,\mathrm{p})]\} \\ &X^{(L)} \le X \le X^{(U)} \\ &d^{(L)} \le d \le d^{(U)} \end{aligned} \tag{10}$$

where $f(x,d,p)$ is the performance or the cost function, μ is the mean value, and ν is one of the dispersion measure operators such as variance *(σ2)* and standard deviation *(σ)*. In addition, x is the vector of uncertain design variables, d is the vector of deterministic design variables, and p is the vector of uncertain parameters that are not design variables.

6. Multi-objective optimization

A hybrid robust multi-objective optimization was used to solve this robust multi-objective optimization problem. This approach has two stages: modified-NSGAII generates a Pareto front, and TOPSIS determines the Pareto front's best solution [17].

Multi-objective optimization is defined as the process of finding a decision variables vector that satisfies constraints and gives acceptable values to all objective functions. Mathematically, in multi-objective optimization, a vector, $X^* = [x_1^*, x_2^*, \ldots, x_n^*]$ should be found to optimize $F_{(x)} = [f_1(x), f_2(x), \ldots, f_k(x)]^T$, subject to m inequality constraints, $g_i(x) \le 0 \ (i = 1 \ to \ m)$and p equality

constraints, $h_j(x) = 0 \ \ (j = 1 \ to \ p)$ where $X^* \in R^n$ is the vector of decision and $F(x) \in R^k$ is the vector of objective functions, both of which must be minimized [21].

The cost functions in multi-objective optimizations are frequently at odds with one another. As a result, there is no one best solution that maximizes all objective functions simultaneously. A set of optimum solutions, known as Pareto optimal solutions or Pareto front solutions, is one solution to these optimization problems [22]. The idea of dominance must be defined before the Pareto optimal solution can be introduced. Assume that x_1 and x_2 are vectors in n-dimensional space and f is a cost function. x_1 is dominated to x_2 if the following conditions are satisfied:

$$\begin{cases} f_i(x_1) \leq f_i(x_2) \ \ (\forall i = 1, \dots, k) \\ and \\ f_i(x_1) \prec f_i(x_2) \ \ (\exists i = 1, \dots, k) \end{cases} \quad (11)$$

A Pareto optimal solution is one that is not dominated by any other solution in the solution space. A Pareto optimum solution cannot be improved in terms of one objective without deteriorating at least another [21]. The Pareto optimum set is made up of all of these non-dominated solutions, and the Pareto front in the objective space is made up of the objective function values. The Pareto front, which consists of Pareto optimum solutions, is the primary goal of multi-objective optimization [13]. The Pareto front, which consists of Pareto optimum solutions, is the primary goal of multi-objective optimization.

7. Robust optimization of friction stir welding parameter

The neural network developed in the previous sections is used in a multivariate robust optimization algorithm using the modified NSGA-II (Non-dominated Sorting Genetic Algorithm) [23]. Also, to determine the performance of Robust optimization, the results of this optimization will be compared with the results of deterministic optimization [17]. In deterministic optimization, uncertainty factors are not considered, and only the main variables are optimized. This MOP was formulated as follows:

$$\begin{cases} Max \ hardness \ (T, R) \\ Max \ tensile \ strenght \ (T, R) \\ 565 \leq Rotational \ Speed \leq 1600 \\ 11 \leq Traverse \ Speed \leq 90 \end{cases} \quad (12)$$

The deterministic Pareto front of two objectives from our previous work has been shown in Fig. 8 [17].

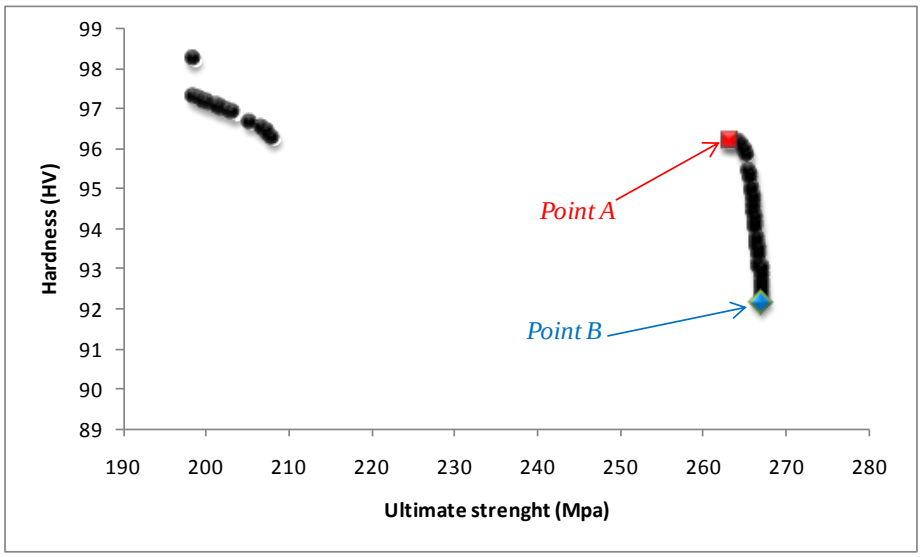

Fig. 8. Pareto front of tensile strength and hardness.

In this figure, point A is introduced as the optimal answer of deterministic multi-objective optimization using TOPSIS results.

Multi-objective optimization was used to find the best friction stir parameters while taking probabilistic objective functions into account. The mean and variance of ultimate tensile strength, and average hardness, have been viewed as objective functions. As a result, the problem of robust optimization can be stated as follows:

$$\begin{cases} Max \ hardness \ (T, R) \\ Max \ tensile \ strenght \ (T, R) \\ Min \ variance \ of \ hardness \ (T, R) \\ Min \ variance \ of \ tensile \ sternght \ (T, R) \\ 565 \leq Rotational \ Speed \leq 1600 \\ 11 \leq Traverse \ Speed \leq 90 \end{cases} \quad (13)$$

In robust design, parameters change in response to previously known probabilistic distribution functions centered on a nominal set of parameters. The uncertain design parameters, namely traverse and rotational speed, are varied with Gaussian distributions within the limits of 3 mm/min and 50 rpm, respectively, in this study. 1000 Monte Carlo assessments utilizing the HSS distribution are used to carry out the evolutionary process of multi-objective optimization. Fig. 9 compares the outcomes of our previous conventional optimization work with the non-dominated individuals of probabilistic optimization in the plane of mean tensile strength and mean hardness [17]. In Figs. 10 and 11, such non-dominated individuals of probabilistic optimization results have been depicted in the other planes. It's worth noting that the four-objective optimization generates a single set of individuals that appear in several objective function planes. Therefore, there are some points in each plane that may dominate others in the same plane. When all four objectives are considered at the same time, however, these individuals are all non-dominant.

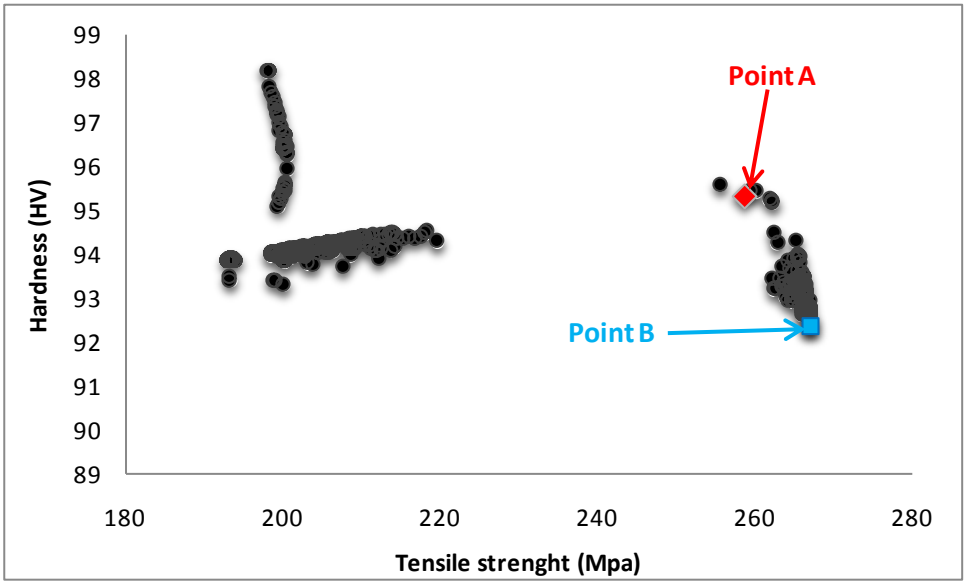

Fig. 9. Mean of tensile strength versus hardness of SEA

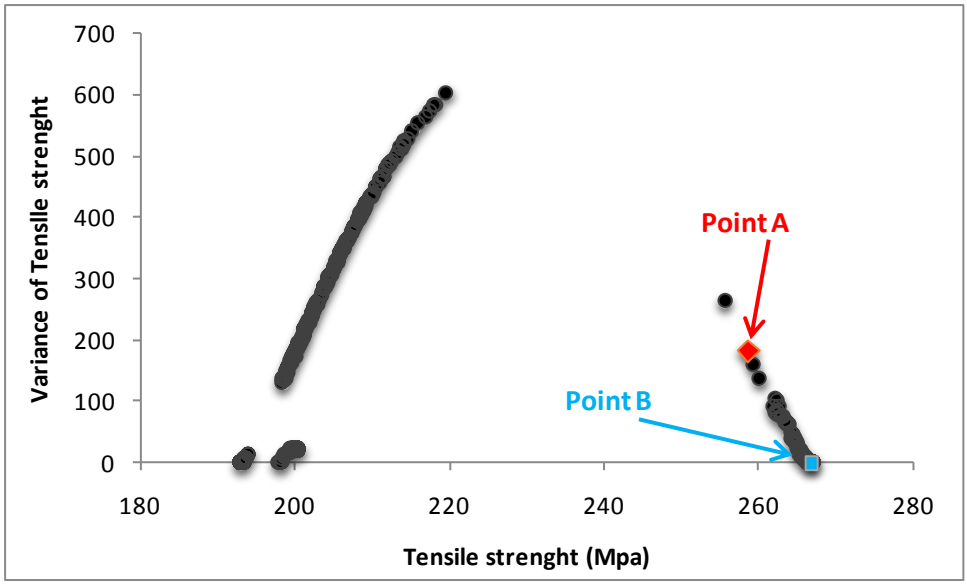

Fig. 10. Variance of ultimate tensile strength versus the mean of ultimate tensile strength in four-objective optimization

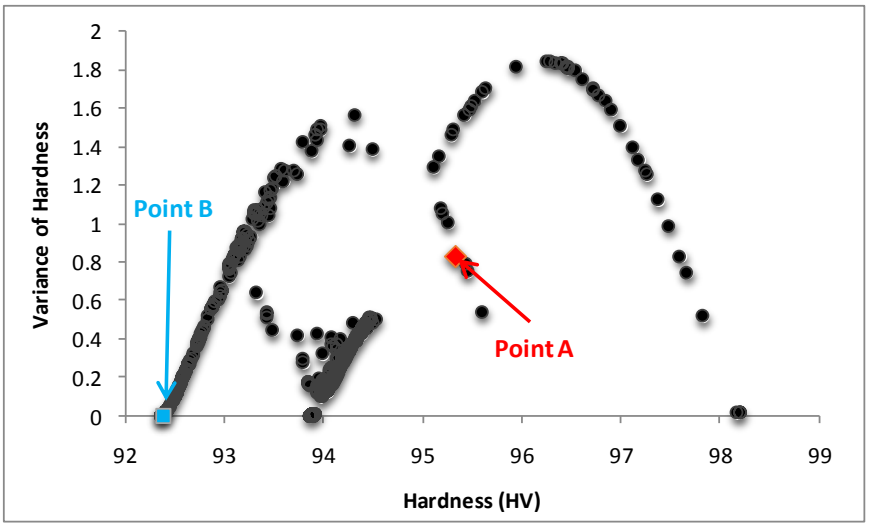

Fig. 11. Variance of hardness versus the mean of hardness in four-objective optimization

Out of all non-dominated four-objective optimization processes compromising all objective functions, it is now wanted to find a trade-off optimum design point. The TOPSIS approach, as stated in Ref. [17], can be used to do this. Individuals obtained from four-objective optimization are subjected to the TOPSIS approach. In this method, non-preference for all objective functions is taken into account using equal weights. As a result, applying TOPSIS to the results of four objective optimization problems yields optimum point B. Figures 9-11 illustrate these points. The probabilistic values of the objective functions for both deterministic point (point A) and probabilistic point (point B) are shown in Table 4.

Table 4. The probabilistic values of functions for both deterministic and probabilistic points.

Optimum point	Rotational Speed (rpm)	Traverse Speed (mm/min)	Mean Tensile strength (Mpa)	The variance of Tensile strength	Mean Hardness (HV)	Variance of Hardness
Point A	1182	11	258.6835	181.8485	95.3171	0.8310
Point B	1467	11	267.0017	1.2341	92.36867	0.00122

Table 3 shows that, in comparison to the previous optimization result, robust optimization produces a far more robust optimal result with roughly the same optimum tensile strength and hardness mean value. Table 5 also compares the deterministic values of the goal functions for trade-off optimum design locations using both deterministic and probabilistic methodologies. Tables 4 and 5 indicate that the probabilistic and deterministic values of the objective functions for the probabilistic point (point B) are nearly comparable. As a result, probabilistic optimization produces a far more reliable optimum solution. For the deterministic point (point A), the probabilistic and deterministic values of the functions disagree. This demonstrates that non-robust and potentially high-risk solutions were obtained without addressing uncertainty.

Table 5. The deterministic values of functions for both deterministic and probabilistic points.

Optimum point	Rotational Speed (rpm)	Traverse Speed (mm/min)	Tensile strength (Mpa)	Hardness (HV)
Point A	1182	11	264.11	95.99
Point B	1467	11	267	92.367

It can also be observed in Fig. 8, and Table 4 and 5 that points B obtained by the probabilistic design approach are placed on the Pareto front of the deterministic design. This means that the design points obtained through robust optimum design are identical to those obtained by deterministic design.

8. Conclusions

In this paper, the mechanical properties of the friction stir welding (FSW) of AA7075-O to AA5083-O aluminum alloys were investigated. First, the mechanical and microstructural properties of the joints produced with different welding parameters were obtained. Experimental results show the joint fabricated, using the FSW parameters of 1400 rpm (tool rotational speed) and 20 mm/min (traverse speed), yielded higher strength properties compared with other joints. The association between the FSW parameters and the mechanical properties of the weld was then successfully modeled using a feed-forward neural network. The obtained models were then used in a robust multi-objective optimization process. To get better results, the standard NSGA-II algorithm was modified. Finally, using the TOPSIS approach to non-dominated solutions, particular trade-off optimum design points were discovered and reported. This study shows that robust optimization provides very more robust optimum results with nearly the same optimum mean value compared to previous optimization results. The results of robust multivariate optimization showed that the rotational speed of 1467 rpm and the traverse velocity of 11 mm/min is the robust optimal process parameters.

Reference

[1] Robitaille, B., et al., Mechanical properties of 2024-T3 AlClad aluminum FSW lap joints and impact of surface preparation. International Journal of Fatigue, 2021. 143: p. 105979.

[2] Sen, M., S. shankar, and S. Chattopadhyaya, Investigations into FSW joints of dissimilar aluminum alloys. Materials Today: Proceedings, 2020. 27: p. 2455-2462.

[3] Dhanesh Babu, S.D., et al., Development of Thermo Mechanical Model for Prediction of Temperature Diffusion in Different FSW Tool Pin Geometries During Joining of AZ80A Mg Alloys. Journal of Inorganic and Organometallic Polymers and Materials, 2021. 31(7): p. 3196-3212.

[4] Eivani, A.R., et al., A novel approach to determine residual stress field during FSW of AZ91 Mg alloy using combined smoothed particle hydrodynamics/neuro-fuzzy computations and ultrasonic testing. Journal of Magnesium and Alloys, 2021. 9(4): p. 1304-1328.

[5] Xu, N., et al., Microstructure and tensile properties of rapid-cooling friction-stir-welded AZ31B Mg alloy along thickness direction. Transactions of Nonferrous Metals Society of China, 2020. 30(12): p. 3254-3262.

[6] Akbari, M. and P. Asadi, Dissimilar friction stir lap welding of aluminum to brass: Modeling of material mixing using coupled Eulerian–Lagrangian method with experimental verifications. Proceedings of the Institution of Mechanical Engineers, Part L: Journal of Materials: Design and Applications, 2020. 234(8): p. 1117-1128.

[7] Akbari, M., P. Asadi, and R.A. Behnagh, Modeling of material flow in dissimilar friction stir lap welding of aluminum and brass using coupled Eulerian and Lagrangian method. The International Journal of Advanced Manufacturing Technology, 2021. 113(3): p. 721-734.

[8] Zhang, J., et al., Improving performance of friction stir welded AZ31/AM60 dissimilar joint by adjusting texture distribution and microstructure. Materials Science and Engineering: A, 2020. 778: p. 139088.

[9] Yuvaraj, K.P., et al., Optimization of FSW tool parameters for joining dissimilar AA7075-T651 and AA6061 aluminium alloys using Taguchi Technique. Materials Today: Proceedings, 2021. 45: p. 919-925.

[10] Han, M.-S., et al., Optimum condition by mechanical characteristic evaluation in friction stir welding for 5083-O Al alloy. Transactions of Nonferrous Metals Society of China, 2009. 19, Supplement 1(0): p. s17-s22.

[11] Amancio-Filho, S.T., et al., Preliminary study on the microstructure and mechanical properties of dissimilar friction stir welds in aircraft aluminium alloys 2024-T351 and 6056-T4. Journal of Materials Processing Technology, 2008. 206(1–3): p. 132-142.

[12] Ghiasvand, A., et al., Effects of tool offset, pin offset, and alloys position on maximum temperature in dissimilar FSW of AA6061 and AA5086. International Journal of Mechanical and Materials Engineering, 2020. 15.

[13] Verma, S. and V. Kumar, Optimization of friction stir welding parameters of dissimilar aluminium alloys 6061 and 5083 by using response surface methodology. Proceedings of the Institution of Mechanical Engineers, Part C: Journal of Mechanical Engineering Science, 2021: p. 09544062211005804.

[14] Khakhali, A., et al., Reliability-based robust multi-objective crashworthiness optimisation of S-shaped box beams with parametric uncertainties. International Journal of Crashworthiness, 2010. 15(4): p. 443-456.

[15] Standard Test Methods for Tension Testing of Metallic Materials, in ASTM E8 / E8M-21. 2021, ASTM International: West Conshohocken.

[16] Akbari, M., et al., The effect of in-process cooling conditions on temperature, force, wear resistance, microstructural, and mechanical properties of friction stir processed A356. Proceedings of the Institution of Mechanical

Engineers, Part L: Journal of Materials: Design and Applications, 2016. 232(5): p. 429-437.
[17] Shojaeefard, M.H., et al., Modelling and Pareto optimization of mechanical properties of friction stir welded AA7075/AA5083 butt joints using neural network and particle swarm algorithm. Materials & Design, 2013. 44(0): p. 190-198.
[18] Akbari, M., et al., Investigation of the effect of friction stir processing parameters on temperature and forces of Al–Si aluminum alloys. Proceedings of the Institution of Mechanical Engineers, Part L: Journal of Materials: Design and Applications, 2015. 232(3): p. 213-229.
[19] Akbari, M., et al., Wear Performance of A356 Matrix Composites Reinforced with Different Types of Reinforcing Particles. Journal of Materials Engineering and Performance, 2017. 26(9): p. 4297-4310.
[20] Khakhali, A., et al., Robust Design of S-Shaped Box Beams Subjected to Compressive Load. Mathematical Problems in Engineering, 2010. 2010.
[21] Etghani, M.M., et al., A hybrid method of modified NSGA-II and TOPSIS to optimize performance and emissions of a diesel engine using biodiesel. Applied Thermal Engineering, 2013. 59(1–2): p. 309-315.
[22] Amanifard, N., et al., Modelling and Pareto optimization of heat transfer and flow coefficients in microchannels using GMDH type neural networks and genetic algorithms. Energy Conversion and Management, 2008. 49(2): p. 311-325.
[23] Jamali, A., et al., Multi-objective evolutionary optimization of polynomial neural networks for modelling and prediction of explosive cutting process. Engineering Applications of Artificial Intelligence, 2009. 22(4–5): p. 676-687.